

# Spectral imaging of near-surface oxygen saturation

Nithya R.Subramanian, John P. Kerekes  
Center for Imaging Science, Rochester Institute of Technology  
54 Lomb Memorial Drive, Rochester, New York  
585-475-6996, 585-475-5988 (fax)  
[kerekes@cis.rit.edu](mailto:kerekes@cis.rit.edu)

Kevin Kearney, Nik Schad  
Geospatial Systems, Inc.  
125 Tech Park Dr., Rochester, New York  
585-427-8310, 585-427-8422 (fax)  
[kevin.kearney@geospatialsystems.com](mailto:kevin.kearney@geospatialsystems.com)

## **ABSTRACT**

A number of non invasive methods have been developed to characterize parameters in near-surface skin tissue; however, the work has usually been concerned with using either spectral or spatial information. This motivated our study in which both spatial and spectral data are used to extract features for characterizing the spatial distribution of near-surface oxygen saturation. This paper addresses combined physical and statistical models to retrieve the ratio of oxy- and deoxy-hemoglobin in tissues from data collected by an imaging spectrometer. To retrieve the oxygen saturation fraction from the data, algorithms from the literature using two or three wavelengths were compared to our new algorithm using the many more wavelengths (25 to 60) available in imaging spectrometer data, and noise reduction achieved through principal component transformations.

In addition to the analysis of experimental spectral imagery, an oxygen saturation phantom of size 128x128 pixels was simulated. In the forward process, a reflectance image was constructed from an assumed oxygen saturation map and the absorption coefficients of oxy-hemoglobin, deoxy-hemoglobin, melanin and other chromophores. The reflectance data have 60 bands spanning 400 nm to 990 nm with 10 nm intervals in the spectral dimension. Varying amounts of white Gaussian noise was added to the reflectance data to simulate measurement errors in an actual experiment. In the backward process, an oxygen saturation image was reconstructed by applying the algorithm to study the effect of measurement error on the retrieved saturation fraction. The resultant images were evaluated by their mean squared error.

Keywords: spectral imaging, oxygen saturation, principal component analysis.

## **INTRODUCTION**

The optical properties of tissues encountered in skin biomedical imaging applications are well known thanks to the efforts of many researchers over the past decades. Although the methods and wavelength range varied greatly, the end result is often the extraction of features such as oxygen saturation in the skin. Additionally, several groups have worked on a number of non-invasive methods to detect and classify abnormal cells. However, the work is usually concerned with extracting either spectral information or the spatial information; only a few researchers have developed a reliable way to combine both the methods to extract effective features for the detection and classification of skin anomalies.

One popular method of analysis of skin tissues is reflectance spectrometry [1-2]. This method has been used to analyze the reflection, absorption and transmission properties of skin tissue when exposed to broadband white-light source. Images collected at selected wavelengths in the range 480nm-720nm have been used to map oxygen saturation of hemoglobin in the dermis of an abnormal cell, which can vary greatly from a normal skin tissue. In [3], reflectance measurements from a hyperspectral imaging system were used for mapping blood oxygen saturation in wounds. The absorption coefficients of oxy-hemoglobin and deoxy-hemoglobin at an oxygen sensitive wavelength (760 nm) and an oxygen insensitive wavelength (800 nm) are utilized by the algorithm.

The potential and limits of multispectral imaging in the diagnosis of cutaneous melanoma is discussed in [4]. In that study, images were collected from 17 selected wavelengths between 420 and 1040nm. Lesion dimension, mean and standard deviation of the lesion reflectance, lesion roundness and border irregularity were found to be the most significant features for successfully classifying benign and malignant melanomas. Validation and improvements of an algorithm for the determination of hemoglobin oxygenations is given in [5]. Erythrocytes are added step by step in a highly scattering media. The hemoglobin concentration in the suspension varied from 0.01 to 1.0 [g hb /dl of suspension], and the oxygenation was changed from 0% to 100% by using a hallow-fiber oxygenator. The light backscattered from the suspension is measured and the hemoglobin oxygenation percentage is calculated by two-flux theory based on the Kubelka-Munk approach. Diffuse Reflectance Spectroscopic Imaging (DRSI) with oblique incidence has also been used to distinguish between benign and cancerous-prone skin lesions [6]. Various features like mean, skewness and Daubechies wavelet entropy were examined to classify the lesions. A region search algorithm was developed to extract 1D and 2D spectral information between 518 and 760nm and a Bayes classifier was then used for classification. Taken together, these publications suggest that the feasibility of obtaining medical diagnostic information from spectral imaging of skin has been established. However, the studies reported have been of relatively small scale, suggesting the large-scale investigation of medical diagnostic effectiveness has not yet been firmly established.

In our research both the spectral and spatial information were taken into account for the analysis of the skin. Both experimental and simulated data sets have been investigated. Two sets of spectral reflectance image data were obtained from Northeastern University [7]. The initial data set was a 300x300 pixel image containing 25 spectral bands spanning from 480 nm to 720 nm and covering an area about 1 inch by 1 inch of a human palm with several landmarks – two parallel veins running across the image, a scratch scar lying in between the two almost parallel veins. The result of the analysis is presented. A second similar data set was recently acquired and processed by our algorithms.

Additionally, several datasets have been acquired by an imaging spectrometer V700 under development at Geospatial Systems, Inc (GSI) [8]. The GSI system mates a Liquid Crystal Tunable Filter (LCTF) together with a 2048x2048 silicon CCD focal plane. It is capable of collecting more than 30 co-registered spectral images spaced every 10 nanometers spanning 400 to 720 nanometers. Example reflectance spectra and retrieved oxygen saturation images are presented for this data set. In spectral images, the reflectance values in the adjacent spectral bands can be significantly correlated. Hence Principal Component Analysis is applied to reduce noise and thereby improve the results.

For the simulation study, a 128x128x60 band reflectance image was generated using a range of oxygen saturation fractions and the known absorption coefficients of oxy-hemoglobin, deoxy-hemoglobin, melanin and other chromophores. The spectral measurements spanned 400 nm to 990 nm with 10 nm intervals. Varying amounts of white Gaussian noise was added to the reflectance to simulate errors occurring in actual data collections.

## Methods and Results

A two layer model of the skin is assumed for the research as shown in Figure 1 below.

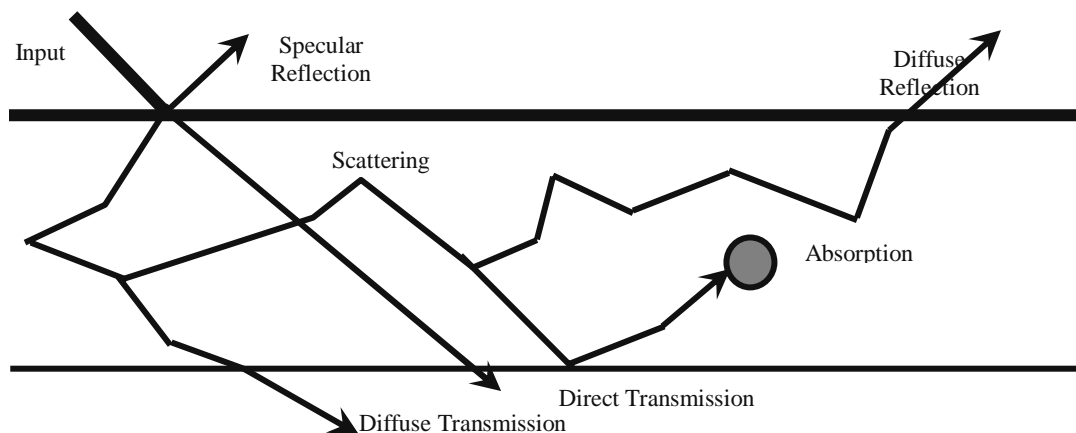


Figure 1. Two layer model of the skin [2].

Lambertian reflectivity is assumed [2]. For a two layer model

$$R=R_0+Te^2R_1 \quad (1)$$

where,  $R_0$ = Reflectance from epidermis  
 $Te$ = Transmission coefficient of epidermis

The reflectance from the dermis,  $R_1$ , is given by

$$R_1 = \frac{\mu_s'}{\mu_s' + \mu_a} \quad (2)$$

here  $\mu_a$  = absorption coefficient  
 $\mu_s' = (1-g)\mu_s$  is the reduced scattering coefficient  
 $g$  = anisotropy obtained by averaging the cosine of the scattering angle.

Absorption co-efficient is given by

$$\mu_a = \mu_{ab} + Csk_o(\lambda) + C(1-s)k_d(\lambda) \quad (3)$$

where  $k_o(\lambda)$  = absorption coefficient of unit concentration of oxy-hemoglobin  
 $k_d(\lambda)$  = absorption coefficient of deoxy-hemoglobin  
 $\mu_{ab}$  = absorption coefficient of other chromophores such as melanin  
 $C$  = Hemoglobin concentration and  
 $s$  = oxygen saturation.

Over a moderate band of wavelengths, the scattering and the absorption coefficients are nearly independent of wavelength. Substituting (3) in (2) we get

$$R_1(\lambda) = \frac{1}{a+bCsk_o(\lambda)+bC(1-s)k_d(\lambda)} \quad (4)$$

hence absorption  $A(\lambda) = \frac{1}{R_1} = a+bCsk_o(\lambda)+bC(1-s)k_d(\lambda) \quad (5)$

If we let  $X= bCs$  and  $Y= bC(1-s)$ , the above equation can be written in matrix form as follows

$$\begin{matrix} \text{A} \\ \left[ \begin{array}{c} A(\lambda_1) \\ A(\lambda_2) \\ \vdots \\ \vdots \\ A(\lambda_{25}) \end{array} \right] \end{matrix} = \begin{matrix} \text{k} \\ \left[ \begin{array}{ccc} 1 & k_o(\lambda_1) & k_d(\lambda_1) \\ 1 & k_o(\lambda_2) & k_d(\lambda_2) \\ \vdots & \vdots & \vdots \\ \vdots & \vdots & \vdots \\ 1 & k_o(\lambda_{25}) & k_d(\lambda_{25}) \end{array} \right] \end{matrix} * \begin{matrix} \text{P} \\ \left[ \begin{array}{c} a \\ X \\ Y \end{array} \right] \end{matrix}$$

Using a pseudo-inverse method the above equation can be solved for the unknowns and the oxygen saturation  $s$  can be determined as shown in equations (6)-(9).

$$A = k * P \tag{6}$$

$$(k^T k)^{-1} * k^T * A = (k^T k)^{-1} * k^T * k * P \tag{7}$$

$$P = \begin{bmatrix} \hat{a} \\ X \\ Y \end{bmatrix} = (k^T k)^{-1} * k^T * A \tag{8}$$

Oxygen saturation  $s = \frac{X}{X+Y}$  (9)

**Noise Reduction through Principal Component Analysis**

In spectral images the reflectance values in the adjacent spectral bands can be highly correlated, while the noise is usually uncorrelated. Hence, Principal Component Analysis (PCA) is applied to reduce noise and thereby improve the results.

Approach

- Covariance of the reflectance is computed
  - Each pixel is a vector of sample data.
  - The dimensionality of the covariance matrix is given by the number of wavelengths in the imaging system.
- Eigenvector and eigenvalue analysis of the covariance matrix is performed.
- Eigenvectors and eigenvalues corresponding to 99% of the cumulative sum of eigenvalues are used for transformation.

Transformed reflectance is given by

$$R'(x,y) = V' * \Lambda' * V'^t * R(x,y) \tag{10}$$

where,  $R(x,y)$  = original reflectance data at pixel location  $(x,y)$

$R'(x,y)$  = transformed reflectance data

$\Lambda'$  = Eigenvalues less than 99% of the cumulative sum

$V'$  = corresponding Eigenvectors

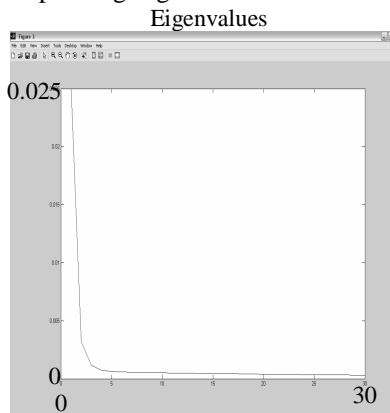


Figure 2(a)

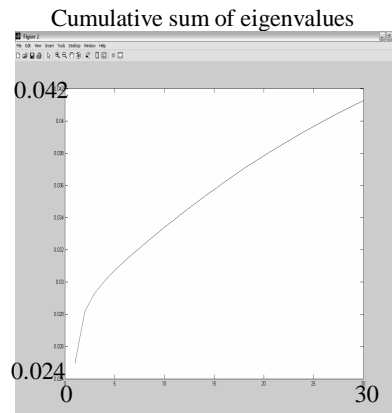


Figure 2(b)

Figure 2(a) shows the plot of eigenvalues of the covariance matrix computed Figure 2(b) shows the cumulative sum of the eigenvalues. Eigenvalues corresponding to 99% of this cumulative sum are taken for the transformation.

The Figure 3 below shows the improvement in the spatial distribution achieved when using the 25 wavelength data and the principal component transformation applied by removing the components with low eigenvalues and transforming back before applying the pseudo-inverse. Quantitative values for the near-surface oxygen saturation fractions were in the reasonable 0.41 to 0.52 range. Other results include  $bC = \frac{1}{Te^2 * \mu s'}$  and  $a = \frac{\mu s' + \mu a_0}{Te^2 * \mu s'}$

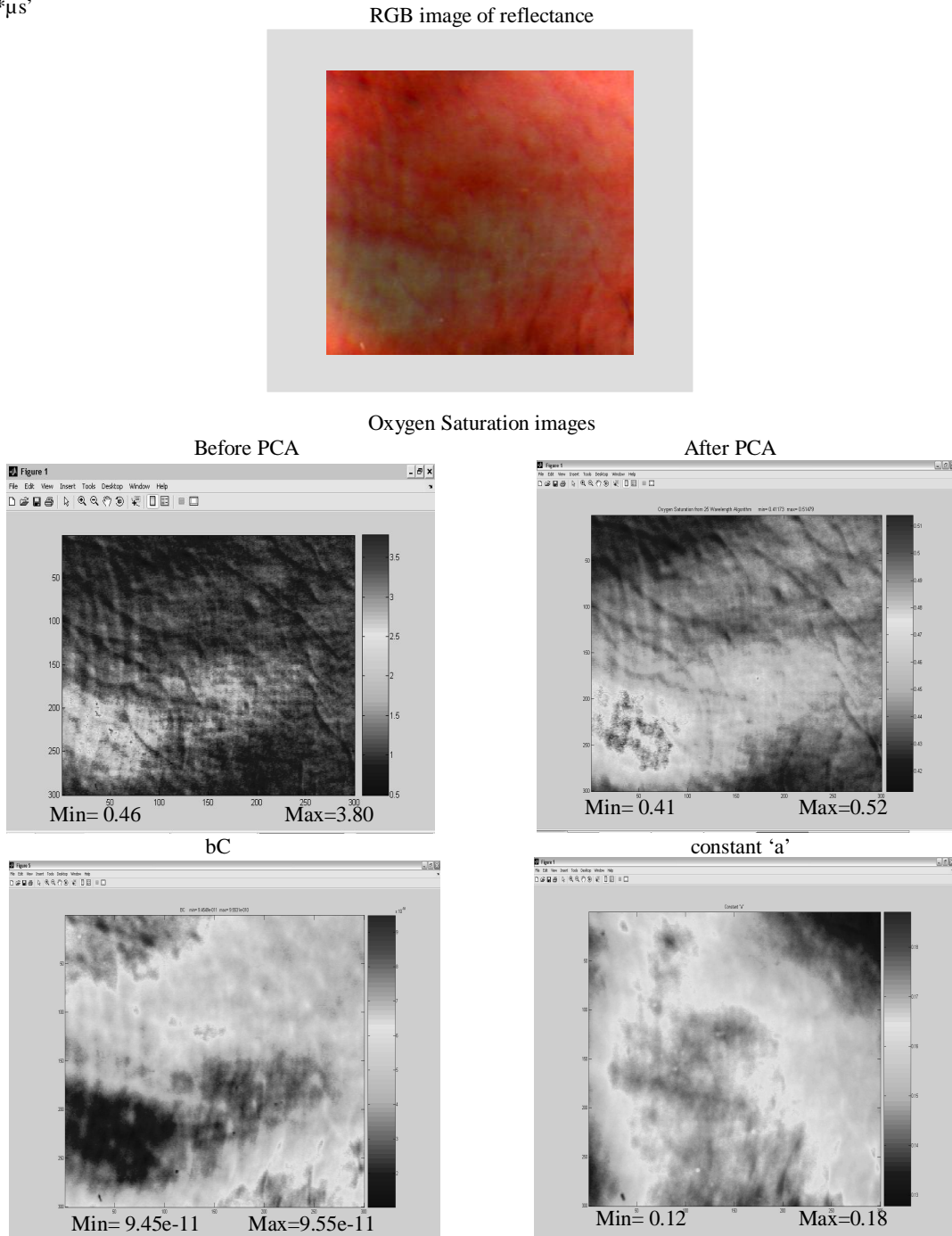


Figure 3. Initial Northeastern University data and results

The above algorithm was also applied to the additional data sets obtained from Geospatial Systems, Inc. and Northeastern University. The oxygen saturation fraction values ranged from -4.03 to 1.82 before PCA and 0.80 to 0.85 after PCA for the Geospatial Systems, Inc data, in Figure 4. For the second set of Northeastern data, the oxygen saturation fraction ranged from 0.22 to 0.46 before PCA and 0.38 to 0.48 after PCA, as shown in Figure 5.

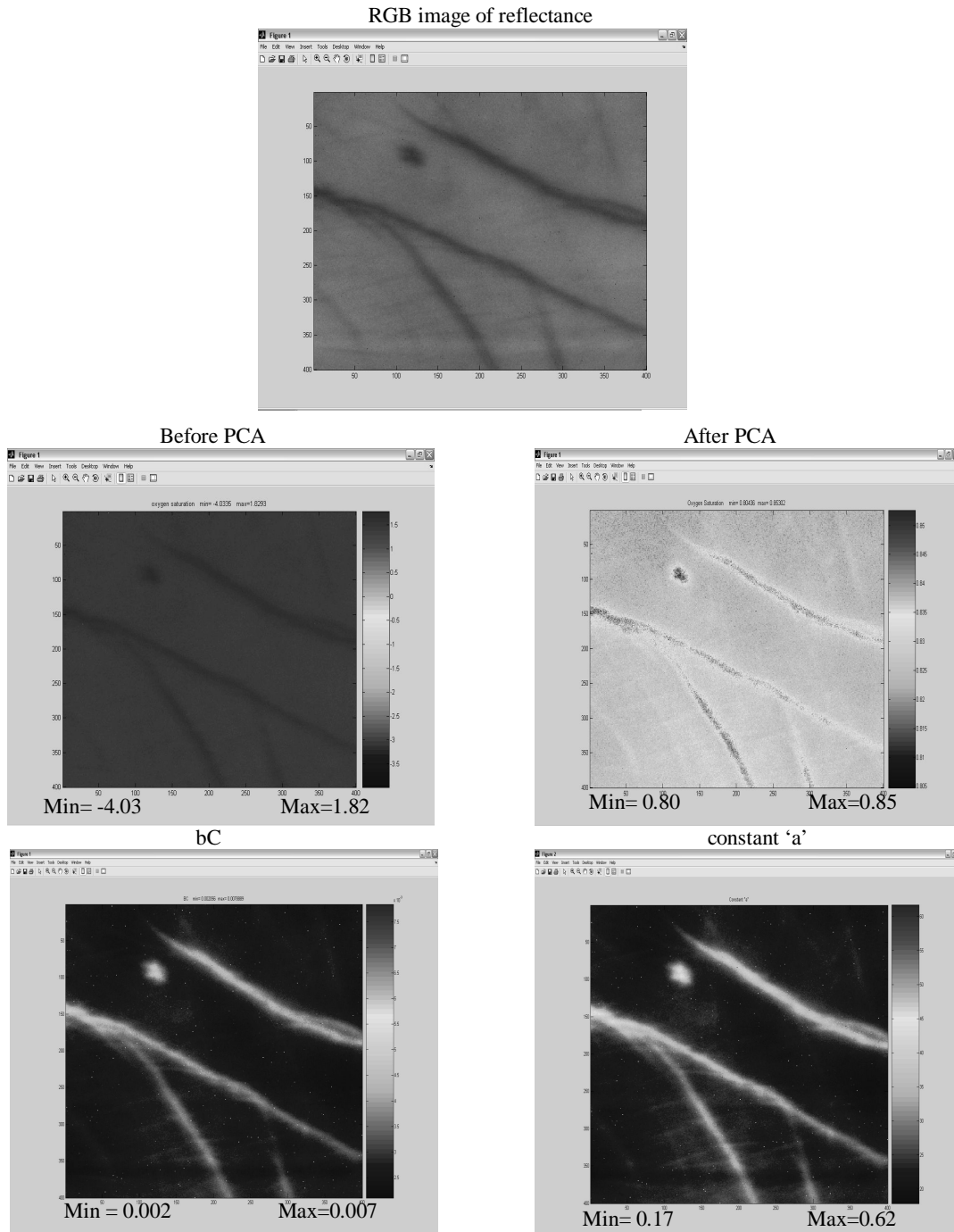


Figure 4. Geospatial Systems, Inc data.

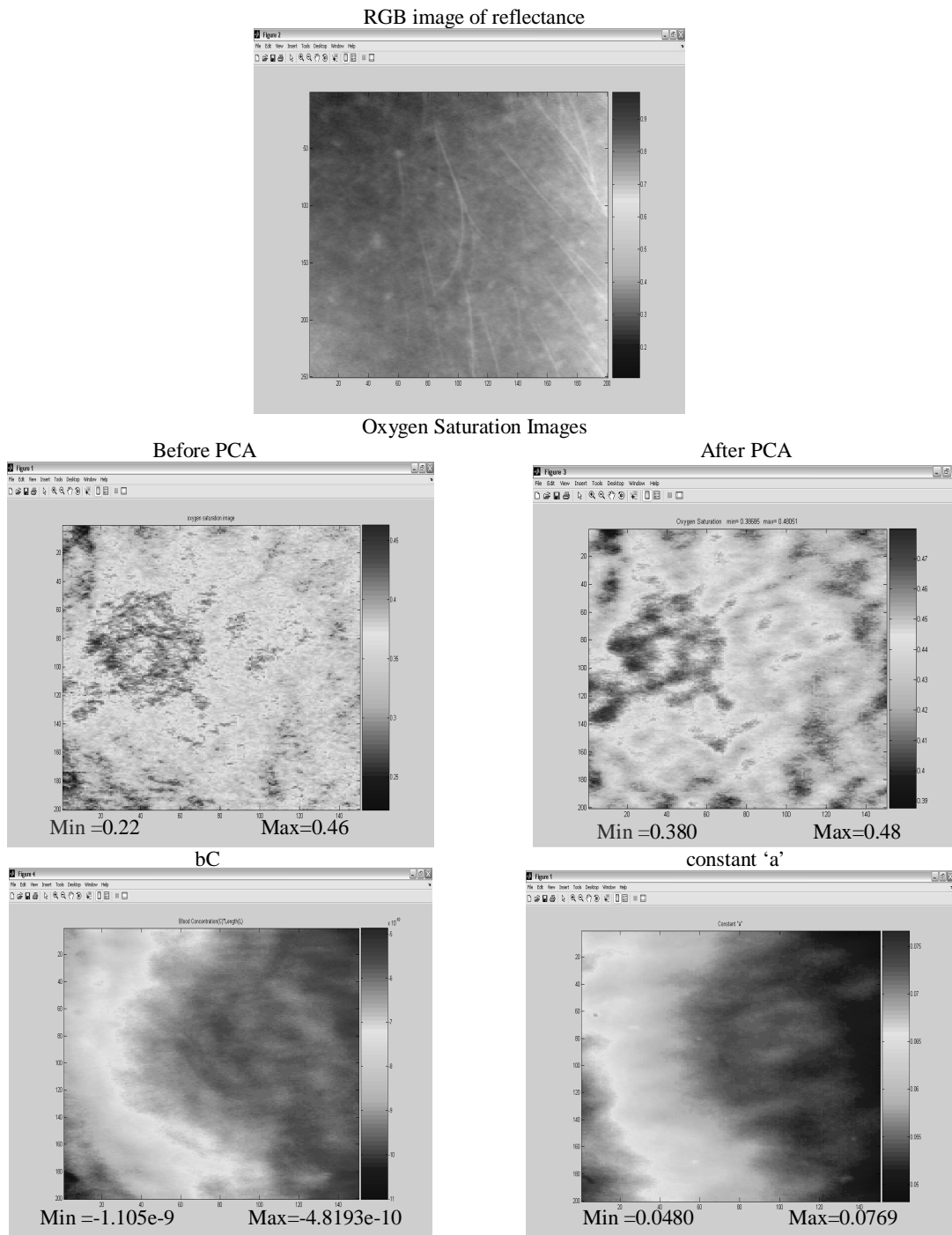


Figure 5. Second set of Northeastern University data.

The quantitative results for the initial dataset from Northeastern University (Figure 3) are shown below in Table 1. The 2 wavelength algorithm uses isosbestic (510nm) and oxygen sensitive (560nm) wavelengths. For the 3 wavelength algorithm, with one fixed wavelength,  $\lambda_2 = 530$  nm, and varying  $\lambda_1$  and  $\lambda_3$ , the determinant of K has the highest magnitude for wavelengths 720 and 560 nm respectively. These three wavelengths are selected as the best choice for determining the oxygen saturation. The 25 wavelength algorithm uses all the wavelengths available in the imaging system (480 nm to 720 nm).

Table 1. Quantitative range of oxygen saturation fractions retrieved for data shown in Figure 3.

Algorithm	Minimum	Maximum
2 Wavelength	1.711	1.721
3 Wavelength	0.766	0.798
25 Wavelength	0.411	0.515

To validate the algorithm, an oxygen saturation phantom of size 128x128 pixels was simulated. In the forward process, a reflectance image was constructed from an assumed oxygen saturation map and the absorption coefficients of oxy-hemoglobin, deoxy-hemoglobin and dermis layer. Reflectance data were generated with 60 bands spanning 400nm to 990nm with 10nm interval in the spectral dimension. Varying amounts of white Gaussian noise was added to the reflectance to simulate measurement noise in the actual experiment with signal-to-noise ratios (SNR) of 10, 100, and 1000. In the retrieval process, the oxygen saturation image was reconstructed by applying several algorithms using 2 wavelengths, 3 wavelengths, 25 wavelengths and all 60 wavelengths. The resultant images are compared by means of their mean square error.

Table 2. Oxygen saturation phantom results for various SNR's and algorithms.

SNR	Algorithm	Minimum	Maximum	RMSE
10	2 wavelength	0.548	0.819	0.334
	3 wavelength	-0.123	0.850	0.111
	25 wavelength	0.005	0.729	0.097
	60 wavelength	0.071	0.822	0.083
100	2 wavelength	0.622	0.769	0.332
	3 wavelength	-0.038	0.798	0.097
	25 wavelength	0.005	0.729	0.095
	60 wavelength	0.003	0.784	0.078
1000	2 wavelength	0.629	0.764	0.332
	3 wavelength	-0.029	0.788	0.098
	25 wavelength	0.005	0.729	0.097
	60 wavelength	0.006	0.780	0.078

## **Conclusion**

In our analyses, the application of the principal component transform reduced the noise in the imaging spectrometer data significantly and improved the stability of the results. The noise sensitivity study using simulated data found a measurement SNR of 100 to be adequate in retrieving the saturated oxygen fraction. The RMSE value decreased as the number of wavelengths used in the algorithm increased. It was observed to be better to use all the wavelengths available in the imaging system instead of 3 wavelengths which may lead to erroneous results if the 3 wavelengths chosen were not appropriate for the given skin image. Additionally, the other constants 'bC' and 'a' were also found for further analysis of the skin.

## **Future Work**

We plan to apply the algorithm to other data sets from Geospatial Systems, Inc and compare the results for different test subjects.

## **Acknowledgement**

The authors acknowledge the support of this project by the Medical Science and Technology Center of the Eastman Kodak Company.

## **References**

- [1] Peter J. Dwyer, Charles A. DiMarzio. "Hyper spectral Imaging for Dermal Hemoglobin Spectroscopy". SPIE Vol 3752, pp 72-82, July 1999.
- [2] Peter J. Dwyer, Charles A. DiMarzio and R. Rox Anderson. "Mapping Blood Oxygen Saturation using a Multispectral imaging system" SPIE Vol. 2976, pp.270-280, 1997.
- [3] Luis Martinez. "A Non-Invasive Spectral Reflectance Method for Mapping Blood Oxygen Saturation in Wounds". Proceedings of the 31st Applied Imagery Pattern Recognition Workshop (AIPR.02).
- [4] B Farina, C Bartoli, A Bono, A Colombo, M Lualdi, G Tragni and R Marchesini. "Multispectral imaging approach in the diagnosis of cutaneous Melanoma: potentiality and limits". Phys. Med. Biol. 45 (2000) 1243–1254.
- [5] Alfons Krug, Manfred Kessler. "Validation and improvements of an algorithm for the determination of hemoglobin oxygenations, based on spectral data recorded by a tissue spectrophotometer". SPIE Vol. 2979. pp. 344-354, 1997.
- [6] Mehru" be Mehru" beo~ lu, Nasser Kehtarnavaz, Guillermo Marquez, Madeleine Duvic, and Lihong V. Wang. "Skin lesion classification using oblique-incidence diffuse reflectance spectroscopic imaging". Applied Optics Vol. 41, No. 1, pp.182-192, January 2002.
- [7] Charles A. DiMarzio and Tianchen Shi, Northeastern University, personal communications, 2005.
- [8] <http://www.geospatialsystems.com/>.